On the Annual Cycle Characteristics of the Sea Surface Height in South China Sea①

Liu Qinyu (刘秦玉), Jia Yinglai (贾英来)

Physical Oceanography Laboratory, Ocean University of Qingdao, Qingdao 266003

Wang Xiaohua (王小华)

School of Geography and Oceanography, University College, University of New South Wales Australian Defence Force Academy, Canberra, Australia

Yang Haijun (杨海军)

Physical Oceanography Laboratory, Ocean University of Qingdao, Qingdao, 266003

(Received August 1, 2000; revised February 27, 2001)

ABSTRACT

The annual cycle characteristics of the SSH in the South China Sea (SCS) are analyzed based on the Sea Surface Height (SSH) anomaly data from the TOPEX / POSEIDON-ERS altimeter data and the Parallel Ocean Climate Model (POCM) prediction. The results show that the distributions of the SSH anomalies of the SCS in January, March and May, are opposite to those in July, September and November respectively; In January (July) there is the SSH negative (positive) anomaly in the deep water basin and at the Luzon Strait, while there is positive (negative) anomaly on the most of continental shelves in the west and south of South China Sea; In March (September) the SSH anomalies are similar to those in January (July), although their magnitudes have decreased and a small positive (negative) anomaly appears in the center of the South China Sea; The amplitude of the SSH annual cycle reaches its maximum in the Northwest of the Luzon Island; The seasonal variability of the wind stress is dominant in the formation of the SSH seasonal variability.

Key words: Sea Surface Height, South China Sea, Monsoon, Parallel Ocean Climate Model

1. Introduction

The South China Sea (SCS) of Southeast Asia is the largest marginal sea in the Northwest Pacific Ocean. It has bottom topography with a mean depth of 1800 m and a maximum depth more than 5400 m. It covers a region from the equator to 23°N and from 99°E to 121°E. The surface area of the SCS is about 3.5 million square kilometers. The deep central basin is enclosed by two extended continental shelves with depth shallower than 100 m. The northern shelf, which also includes the area of South China and Gulf of Tonkin, extends from Taiwan southwestward to 13°N. On the north shelf, the exchange of water between the SCS and the East China Sea occurs through the Taiwan Strait, which has a sill depth of 60 m. The southern shelf consists of Gulf of Thailand and Sunda Shelf between Malay Peninsula and Bruni. The Sunda Shelf is connected to the Java Sea and the Indian Ocean through the Strait of Malacca. The Philippines and Palawan separate the SCS from the Pacific Ocean on

①The work was supported by the NSFC (No. 49636230) and National Key Program for Developing Basic Science (G1999043807) of Ministry of Science and Technology of China.

the east side, where the continental slope is steep with practically no continental shelf. There are three openings on the eastern boundary. The widest and deepest is the Luzon Strait, which is the major pathway of the Pacific water to the deep basin. Two narrower passages to the north and south of the Palawan Island connect the SCS to the Sulu Sea. Since the SCS is in the region of the East Asian monsoon, the characteristics of circulation in SCS are determined mainly by the seasonal variability of the monsoon.

The seasonal variability of SSH in the South China Sea has been analyzed by Ho et al. (2000) using TOPEX / POSEDON (T / P) altimeter measurements along 16 ground tracks, and it has been pointed out that the SSH images are generally characterized by a sea surface tilting downward to east (west) in winter (summer) and a single high sea level peak centered at 14°N,114°E in spring. But the formation mechanism of the seasonal variability of the SSH has not been discussed in detail and many isolines of SSH near coast were crossed with coast in Ho et al. (2000).

According to the SCS monthly mean wind stress curl during the period of 1950–1992, the basin scale Sverdrup transport in SCS is calculated and the basic seasonal features of the Sverdrup circulation are obtained by Liu et al. (2001a). The distribution patterns of the Sverdrup circulation anomaly are opposite between the months of each half year, because the monthly mean wind stress curl anomaly is opposite between the months of each half year. It suggested that the seasonal variability of the Sverdrup circulation is a cycle with a period of about one year forced by monsoon in SCS. But the Sverdrup circulation is only a part of the circulation in the SCS, because, besides the sea surface wind, the surface buoyancy flux and the kuroshio current also have effects on the SSH and the circulation. In order to understand the seasonal variability characteristics of the SSH and circulation in the SCS, the comparison study between the observational data and output data of OGCM is very important.

In this paper, based on the TOPEX / POSEDON–ERS altimeter data , SSH prediction from high resolution Parallel Ocean Climate Model (POCM) and the Levitus data, we will study seasonal changes of the SSH and to understand the SSH annual cycle formation mechanism in the SCS.

2. Data

2.1 *Maps of sea surface height anomaly altimeter data products*

Maps of Sea Surface Height Anomaly (MSSHA) altimeter data products are generated using the following data sets: AVISO GDR–M products for TOPEX / POSEIDON (T / P) and CERSAT OPRs for ERS altimeter data (35–day repeat orbit periods). The MSSHA altimeter products are generated by the CLS Space Oceanography Division as part of the European Union Environment and Climate project AGORA (ENV4–CT9560113) and DUACS (ENV4–CT96–0357). The " Anomaly" means that the data do not include the climate average of the SSH.

The MSSHA products are available every 10 days with a $0.25° \times 0.25°$ resolution. Data products are between October 22, 1992 and January 24, 2000 every 10 days and there are data during the ERS–1 ice monitoring and geodetic missions, i.e. no files available between December 26, 1993 and March 31, 1995. The monthly mean anomalies of the SSH have been calculated based on the above data from MSSHA in this paper.

2.2 *SSH from POCM simulation*

POCM has a horizontal resolution of 0.25° and 20 layers in vertical. The model has a free surface, which is used to predict the SSH (Semtner, 1992). Because the POCM is a global OGCM, the SSH prediction in SCS from the POCM could not be affected by the open boundary conditions, for example the flow in the Luzon strait. Stammer et al. (1996) compared the POCM SSH prediction with the SSH from T / P altimeter data. He found that the agreement between the two is reasonable both in the SSH spectral distribution, and in the SSH amplitude and phase of the annual cycle in the global oceans. Li et al. (1998) also concluded that both the SSH rms and the locations of maximum / minimum core from the POCM compared well with those from the T / P data respectively. We will use 10–day averaged Sea Surface Height (SSHA) from POCM and T / P (3 October 1992–9 October 1996) to study the seasonal variability of the SSH in the SCS in this paper.

3. Annual cycle of the SSH in the SCS

3.1 *Seasonal variation*

The monthly mean SSHAs from the POCM and the MSSHA have been shown in Fig. 1 and Fig. 2. Comparing both the monthly mean SSHAs, there is almost no difference between them in pattern and intensity, except in off–coast.

In January, from the POCM (Fig. 1) and the MSSHA (Fig. 2) it is shown that the SSHAs in the whole basin in winter are negative, and the SSHAs are positive in the shallow shelf. There is a cyclonic circulation in the whole basin and surrounded by this circulation are the two cyclonic eddies in the north (115°E, 16°N) and the south (112.5°E, 10°N) of the SCS. The northern negative center is larger in area than the southern one. The negative anomaly in the north with a minimum of −12 cm corresponds to the center of Luzon Cold Eddy (Yang and Liu, 1998a, b). The Luzon Cold Eddy is the strongest in the year. This pattern is similar to the result from Sverdrup circulation (Liu et al. 2001a) and from observational analysis results of the T / P data along orbital by Ho et al. (2000) and the Dynamic Height by Xu et al. (1980). On the western and southern continental shelves, the SSH anomalies are positive, which is clearly due to the Ekman transport under northeast wind in winters and the shallow shelf.

In March the SSH anomalies are similar to those in January, although their maximum have decreased (from POCM result). From MSSHA (Fig. 2), the minimum of the negative anomaly (−12 cm) moved further northeast to the location of 119°E, 18°N, but there is positive SSHA center appears around 112.5°E, 15°N. This is caused by the change of the wind stress curl from positive to negative there, which produces an anti–cyclonic circulation in the center of the SCS and by the increasing of net heat flux in March (Yang et al., 1999). This presentation of the anti–cyclonic circulation is advantageous to the SST positive anomaly, because the cold water is suppressed in the center of the anti–cyclonic circulation (Liu et al., 1997).

In May, the westward–extended subtropical high often controls the SCS, with a clearer weather and higher solar radiation. The temperature of the upper layer of the SCS increases dramatically (Yang and Liu, 1998b). The SSH anomalies start to become positive in the deep water basin, which is similar to the Sverdrup circulation in spring (Liu et al., 2000) and the SSH in May from Ho et al. (2000). A maximum SSH positive anomaly is 6 cm and located at 115°E, 15°N from both the POCM and MSSHA. However, the SSH anomalies in the

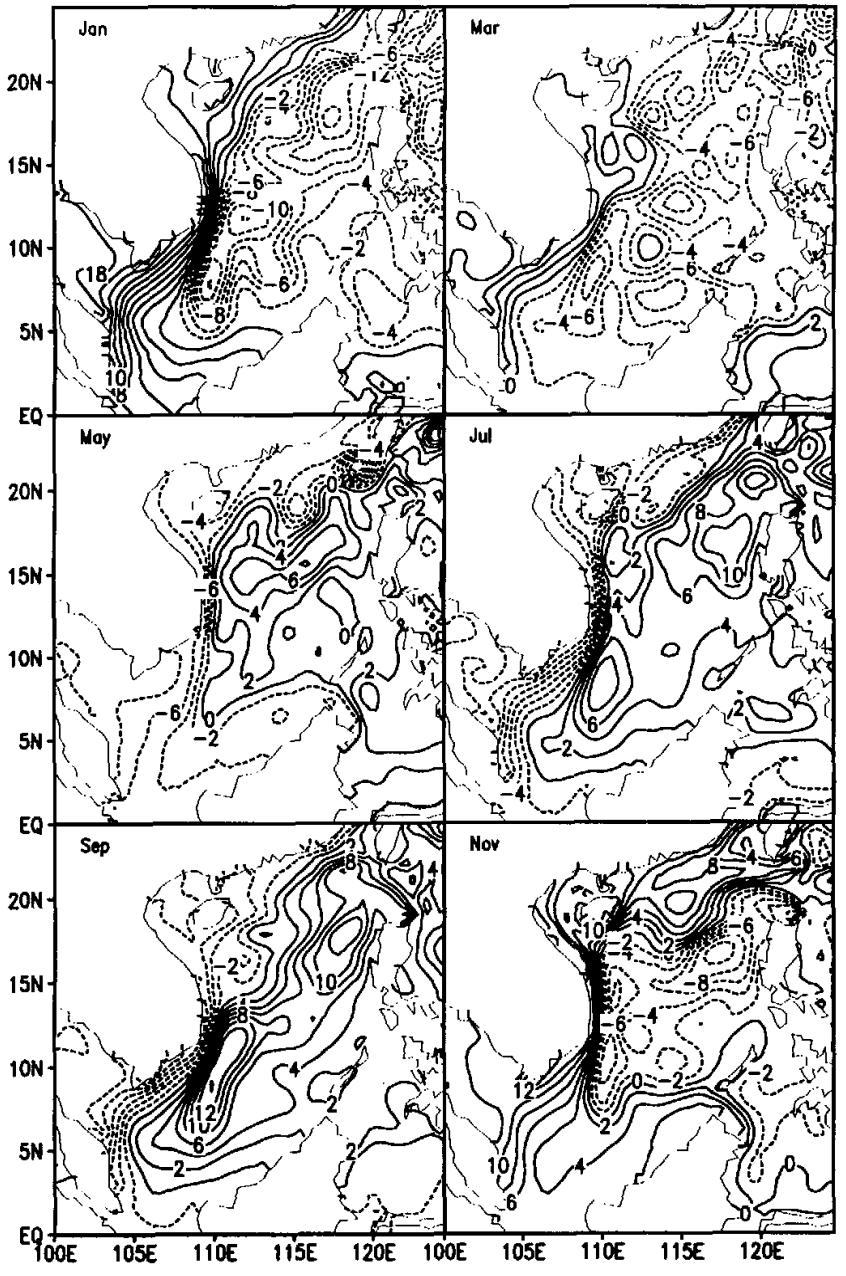

Fig. 1. The monthly averaged SSHA in the SCS from POCM simulation.

southern and northern SCS and on its western continental shelf become negative from positive in winter. This suggests that the Ekman transport towards these regions disappears because the winter monsoon no longer exists.

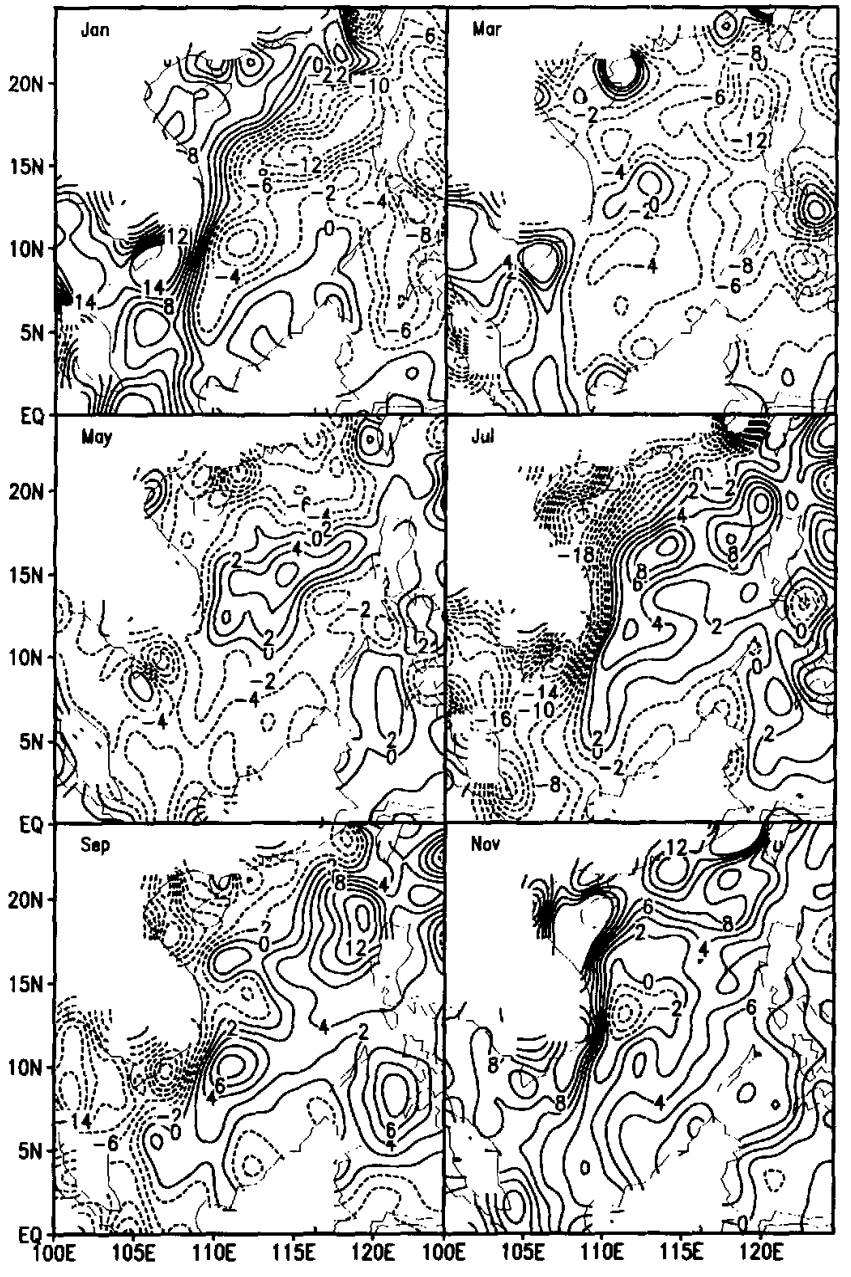

Fig. 2. The monthly averaged SSHA in the SCS from MSSHA (observational data).

In July the summer monsoon is the dominant wind over the SCS. In contrast to January, the positive SSH anomalies are larger in the deep basin with a maximum value reaching 10 cm in the west and northwest of the Luzon Island from MSSHA data and POCM simulation

data (Fig. 1 and Fig. 2). On the continental shelves, the SSH anomalies are negative. There is another maximum of the SSHA, which is located around 110°E, 8°N from the POCM simulation result, and there are still two maxima of the SSHA, which is located in the same places as that from MSSHA but it does not exist in Ho et al. (2000). Corresponding to two positive anomaly centers of the SSH there is an anti-cyclonic circulation anomaly with basin scale. Those positive anomaly maxima of SSH are due to the negative centers of the wind stress curl anomaly, and similar pattern of SSHA was found in Xu et al. (1980). In contrast to January, on the western and southern continental shelves, the SSH anomalies are negative and it is positive in the east of the SCS from the POCM prediction and MSSHA observation, which is clearly due to the Ekman transport under southwesterly. It means that the sea surface wind curl and its Ekman transport are dominant control fact in the formation of the SSH pattern in July.

In September the SSH anomalies are similar to those in July, but opposite to those in March. There are positive anomalies in the deep basin with maximum values reaching 12 cm from both data and it is located northwest of the Luzon Island. The two maxima centers of the SSHA and the anti-cyclonic circulation with the basin scale still subsist. As the SCS eastern boundary consists of several straits, the summer monsoon cannot generate as much water mass accumulation along the eastern boundary as that along the western boundary during the winter monsoon. However, from Fig. 1 and Fig. 2 it is obvious that there are positive SSHAs in southeast of the SCS. It also shows that there is a maximum mass accumulation at the western side of the Luzon Island, which is similar to the analysis result of Ho et al. (2000) in September.

In November, the monsoon again changes its direction. The distribution of the SSHA is opposite to that in May. There appear negative anomalies in the deep basin, with a minimum of −10 cm (POCM) or −8 cm (MSSHA), but the negative anomalies area is smaller from the MSSHA than that from the POCM. In the north and south of these negative SSH anomalies, there are positive SSH anomalies in the SCS, whose pattern is similar to the Sverdrup circulation in fall (Liu et al., 2001a) and SSH image in middle SCS from Ho et al. (2000). The SSH anomalies in November are again determined by its surface wind stress curl distribution over the SCS, because there is positive wind stress curl in the deep basin during November.

To conclude, the distributions of the SSH anomalies in January, March and May are opposite to those in July, September and November respectively. During the winter monsoon, water mass transport against the west coast of the SCS is stronger than that against the eastern coast in summer monsoon. In the deep water basin, the strongest seasonal variation in the SSH anomalies appears near the northwest of the Luzon Island (116°E, 18°N), which is the lowest (< -12 cm) in January and March, and the highest (> 10 cm) in July and September, and another stronger seasonal variation of the SSH appears near 112.5°E, 10°N, in which the SSHA is about−10 cm in winter and above 8 cm in July and September.

3.2 *The SSH oscillation*

In order to further study the characteristics of the SSH seasonal variability, we compared the SSHA at 116°E and 18°N, where the maximum SSH variability is observed, with the SCS area averaged SSHA from October 1992 to October 1996 (Fig. 3). The comparison of the two anomalies indicates: (a) The time series of the SSHA and its running mean at 116°E and 18°N are almost the same in phase with the area averaged time series of the SSHA in all of the SCS, although some small difference exists in their amplitudes. (b) The SSH oscillation has a main period of one year. For the most part of SCS, the SSH anomalies are negative from

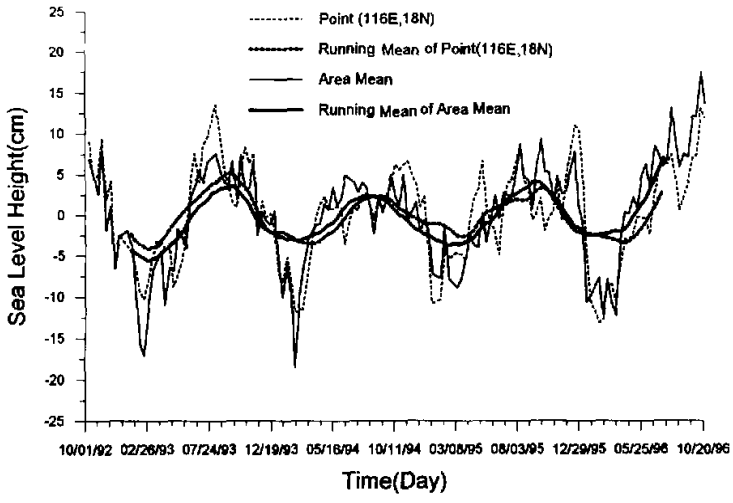

Fig. 3. Time series of the SSH at 116°E and 18°N (solid line) and area averaged SSH over entire SCS (dashed line). The corresponding running mean is three-point (about 30 days) sleek average.

November to next May, the anomalies change to positive during the rest of the cycle.

4. The annual cycle formation mechanism of the SSH in the SCS

To further examine the formation mechanism of the SSHA, the total steric height (0–1000 m) is calculated (Liu et al., 2001b) using the Levitus data (1982). The seasonal anomalies are calculated and shown in Fig 4a.

Based on the Levitus data analysis, the mean depth of the upper boundary of the thermocline is about 50 m (Shi et al., 2001; Liu et al., 2000), and its depth is shallower than 50 m in the northwest (southeast) of the SCS during summer (winter). The seasonal variation maximum of the mixed layer depth is about 20 m in the SCS. We support that the mean depth of the mixed layer is the effective depth of the surface buoyancy flux forcing. Then the anomalies of the surface steric height are calculated using the Levitus data for the upper 50 m (Levitus 50) (Liu et al., 2001b).

In the seasonal variation of total steric height (0–1000 m), there also exists wind effect and others except the buoyancy flux. The smallness of the SCS ocean basin, however, does make the annual variability in the SCS different from that in large oceans. With the wave speeds of 40 cm s^{-1} to 10 cm s^{-1}, the planetary wave crosses the SCS (of about 1000 km) in 1 to 4 months. This short thermocline adjustment time implies that the forced planetary wave response degenerates into a quasi-steady response in seasonal mean (Liu et al., 2001b), therefore, in the lowest order, the baroclinic fields are in the quasi-steady baroclinic Sverdrup balance. It means when Ekman pumping is positive (negative), the thermocline rises (sinks) and the temperature under 50 m decreases (increases), then the steric height under 50 m would decrease (increase) and the negative (positive) anomaly of the steric height under 50 m would appears. Therefore the difference between total steric height and Levitus 50 can reflect the effect of the Ekman pumping, and can be as the dynamic height by wind. The most striking

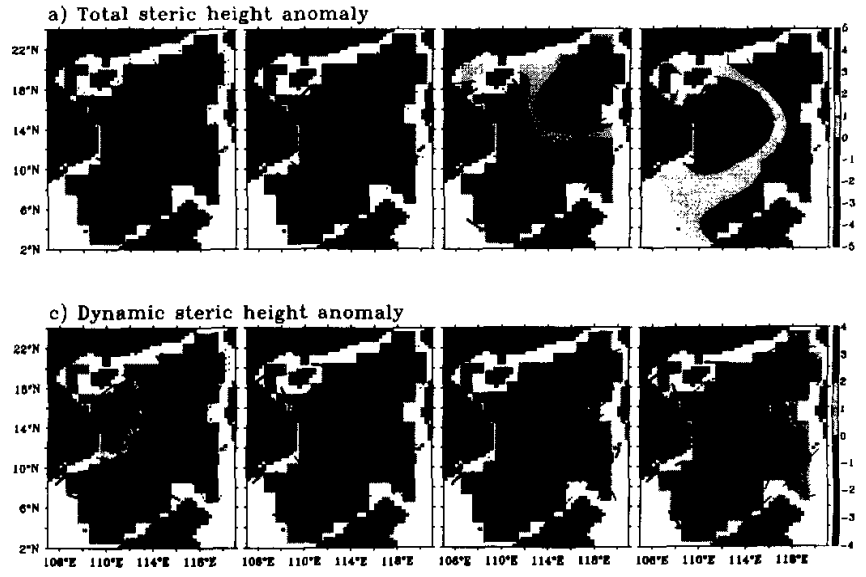

Fig. 4. Steric height anomaly (cm) from Levitus T& S(1982). (a) the total, (b) dynamic steric height anomaly.

feature in Fig. 4 is the agreement of the spatial patterns between the dynamic steric height anomaly fields and the total steric height anomaly in all of the seasons, especially in the central SCS. The summer and fall patterns look like the inverses of the winter and spring patterns respectively. The dynamic steric height amplitude (Fig. 4b) is almost similar to the total (Fig. 4a); then the wind effect is very important in the seasonal variation of the SSH in the SCS.

The discussion above leads to an important conclusion: the observed annual cycle of dynamic SSH with its implied upper oceanic circulation represents the response of baroclinic planetary waves to the Ekman pumping, which can be understood from the seasonal evolution of the upper ocean Sverdrup flow (Liu et al., 2001a).

5. Conclusions

The above analysis leads us to conclude that:

1) The SSH variability has a clear seasonal cycle in the SCS. The distributions of the SSH anomalies in January, March and May are opposite to those in July, September and November respectively. In January (July) SSH anomalies are negative (positive) in the deep basin and at the Luzon Strait, while they are positive (negative) on most of the continental shelves in the west and south of the South China Sea. In March (September) the SSH anomalies are similar to that in January (July). Some small positive (negative) anomalies appear in the middle of the South China Sea. The sign of the SSH anomalies changes from

negative (positive) to positive (negative) in May (November), while the SSH anomalies in the northern and southern parts of the deep basin and on the west coast continental shelf change from positive (negative) to negative (positive).

2) There are two variation centers in SSH anomalies in the SCS, while the strongest seasonal variability in the SSH anomalies is near 116°E, 18°N and the other is near 112.5°E, 10°N.
3) The time series of the SSHA and its running mean at (116°E, 18°N) are almost the same in phase with the area averaged time series of the SSHA in all of the SCS, although some small difference exists in their amplitudes.
4) Because the seasonal mean SSH and the wind curl are in the Sverdrup balance, the forced response is dominant in seasonal mean of SSH. In the formation of the SSHA seasonal variation the wind effect is very important.

The authors would like to thank Dr. Robin Tokmakian and Peter Braccio for providing the CD-ROM with the data of POCM.

REFERENCES

Chao, S. Y., P. T. Shaw, and J. Wang, 1995: Wind relaxation as a possible cause of the South China Sea Warm Current. *Journal of Physical Oceanography*, **51**, 111–132.

Ho, C. R., Q. Zheng, Y. S. Soong, N. J. Kuo, and Jian-Hua Hu, 2000: Seasonal variability of sea surface height in the South China Sea observed with TOPEX / Poseidon altimeter data. *J.Geophys. Res.* **105(C6)**, 13981–13990.

Levitus, S., 1982: *Climatological Atlas of the World Ocean*. NOAA Prof. Pap. No.13. U. S. Government Printing Office, Washington, DC, 177 pp.

Li, W., Q. Liu, and H. Yang, 1998: On the characteristics of the circulation in the Luzon Strait. *Journal of Ocean University of Qingdao*, **28**, 345–351 (in Chinese).

Liu, Q., W. Li, and Q. Xu, 1997: On the interaction of northeast monsoon and South China Sea circulation. *Chinese Journal of Oceanology and Limnology*, **28**, 493–502 (in Chinese).

Liu, Q., H. Yang, and Q. Wang 2000: Dynamic characteristics of seasonal thermocline in the deep sea region of the South China Sea. *Chin. J. Oceanol. Limnol, 2000*, **18(2)**, 104–109.

Liu, Q., H. Yang, and Z.Y. Liu, 2001a: Seasonal feature of the Sverdrup circulation in the South China Sea. *Progress in Natural Science*, **11(3)**, 203–206.

Liu, Z. Y., H. J. Yang, and Q. Y. Liu, 2001b: Regional dynamics of seasonal variability of sea surface height in the South China Sea. *J. Phys. Oceanogr.*, **31(1)**, 272–284.

Semtner, A. J. Jr., and R. M. Chernin, 1992: Ocean general circulation from a global eddy-resolving model. *J. G. R.*, **97**, 5493–5550.

Shi P., Y. Du, D. Wang, and Z. Gang, 2001: Annual cycle of mixed layer in South China Sea. *Journal of Tropical Oceanography*, **20(1)**, 1–8 (in Chinese).

Stammer, D. C., R. Tokmakian, A. J. Semtner, and C. Wunsch, 1996: How well does a 1 / 40 global circulation model simulate large-scale oceanic observations? *Journal of Geophysical Research*, **10**, 25,779–25,811.

Xu X. Z., Qiu Z., and Cheng, H. C., 1980: A survey of the circulation of the SCS. *Proceedings of the Chinese Oceanography and Limonology Conference on hydrological meteorology*, 137–145 (in Chinese).

Yang, H. J., and Q. Y. Liu, 1998a: A review on the South China Sea circulation study. *Earth Science Progress*, **13**, 364–368 (in Chinese).

Yang, H. J., and Q. Y. Liu, 1998b: On the seasonal characteristics of the South China Sea surface temperature. *Oceanology and Limnology*, **29(5)**, 501–507 (in Chinese).

Yang, H. J., Q. Y. Liu, and X. J. Jia, 1999: On the upper oceanic heat budget in the South China Sea: Annual Cycle. *Advances in Atmospheric Sciences*, **16(4)**, 619–629.

南海海平面高度年循环的特征

刘秦玉 贾英来 王小华 杨海军

摘 要

根据 TOPEX / POSEIDON-ERS 高度计提供的海平面高度异常资料和并行海洋气候模式(POCM)模拟海平面高度资料，分析了南海海平面高度年循环特征。结果表明：1 月，3 月和 5 月海平面高度的异常值分别与 7 月，9 月，11 月的异常值相反。1 月(7 月)，深水海区与吕宋海峡的海平面高度为负(正)异常，在大部分陆架区和南海的西和南部，海平面高度为正(负)异常。在 3 月(9 月)，除海平面高度异常的量级已减少，且较小的 SSH 正异常(负异常)出现在南海的中部以外，海平面高度异常的分布型与 1 月(7 月)类似；SSH 的年循环的最大振幅出现在吕宋岛的西北海域；风的季节变化是南海 SSH 季节变化的主要原因。

关键词：海平面高度，南中国海，季风，并行海洋气候模式